Int J Comput Vis (2009) 84: 113–129
DOI 10.1007/s11263-008-0133-9

New Possibilities with Sobolev Active Contours

Ganesh Sundaramoorthi · Anthony Yezzi · Andrea C. Mennucci · Guillermo Sapiro

Received: 30 September 2007 / Accepted: 14 March 2008 / Published online: 26 July 2008

Abstract Recently, the Sobolev metric was introduced to define gradient flows of various geometric active contour energies. It was shown that the Sobolev metric outperforms the traditional metric for the same energy in many cases such as for tracking where the coarse scale changes of the contour are important. Some interesting properties of Sobolev gradient flows include that they stabilize certain unstable traditional flows, and the order of the evolution PDEs are reduced when compared with traditional gradient flows of the same energies. In this paper, we explore new possibilities for active contours made possible by Sobolev metrics. The Sobolev method allows one to implement new energy-based active contour models that were not otherwise considered because the traditional minimizing method render them ill-posed or numerically infeasible. In particular, we exploit the stabilizing and the order reducing properties of Sobolev gradients to implement the gradient descent of these new energies. We give examples of this class of energies, which include some simple geometric priors and new edge-based energies. We also show that these energies can be quite useful for segmentation and tracking. We also show that the gradient flows using the traditional metric are either ill-posed or numerically difficult to implement, and then show that the flows can be implemented in a stable and numerically feasible manner using the Sobolev gradient.

Keywords Active contours · Gradient flows · Sobolev norm · Global flows · Shape optimization · Shape priors · Ill-posed flows

1 Introduction

Active contours (Kass et al. 1987) is a popular technique for the segmentation problem. Over the years there has been a progression of active contours derived from edge-based energies (e.g., Caselles et al. 1993, 1995; Malladi et al. 1995; Kichenassamy et al. 1995), to region-based energies (e.g., Mumford and Shah 1985, 1989; Ronfard 1994; Zhu et al. 1995; Yezzi et al. 1999; Paragios and Deriche 2000, 2002; Chan and Vese 2001), to more recently, prior-based energies (e.g., Leventon et al. 2000; Tsai et al. 2001; Cremers and Schnörr 2001; Chen et al. 2002; Rousson and Paragios 2002; Cremers and Soatto 2003; Raviv et al. 2004) and energies incorporating complex geometrical information (e.g., Kim et al. 2002; Rochery et al. 2003; Nain et al. 2004; Sundaramoorthi and Yezzi 2005; Guyader and Vese 2007). The progression from simple to more complicated energies is not only due to a desire to segment more complicated images, but it can also be attributed to the traditional gradient descent technique becoming trapped by (undesirable) local minima of the energy being optimized. Therefore there have been efforts to design optimization schemes that can obtain the global minimum curve or at least a better local minimum of a generic energy. For example, the minimal path technique

Sundaramoorthi and Yezzi were supported by NSF CCR-0133736, NIH/NINDS R01-NS-037747, and Airforce MURI; Sapiro was partially supported by NSF, ONR, NGA, ARO, DARPA, and the McKnight Foundation.

G. Sundaramoorthi (✉) · A. Yezzi
School of Electrical Engineering, Georgia Institute of Technology, Atlanta, USA
e-mail: ganeshs@ece.gatech.edu

A.C. Mennucci
Scuola Normale Superiore, Pisa, Italy

G. Sapiro
Dept. of Electrical and Computer Engineering, University of Minnesota, Minneapolis, USA

(Cohen and Kimmel 1996) was designed to find the global minimal solution of the edge-based energy considered in Caselles et al. (1995), Kichenassamy et al. (1995). Another technique, called graph cuts (Boykov and Jolly 2001; Kolmogorov and Boykov 2005), was designed for minimizing discrete approximations to certain active contour energies.

The limitation of these global methods is that they may be applied to only certain types of energies, and therefore gradient descent methods must be used in many cases. Moreover, for many applications (e.g. object tracking), it is beneficial to incorporate the information from an initial contour (e.g. the contour from the previous frame for object tracking) to find the contour of interest. In such cases, typically for speed considerations, simple energies are considered for which a global minimum is not always desired, but rather a local minimum contour "close" to the initial contour is desired. For such cases gradient descent methods are ideal. Recently, Michor and Mumford (2006), Yezzi and Mennucci (2005a, 2005b), Charpiat et al. (2005) have noticed that the gradient of an energy that is used in descent algorithms depends on a metric chosen on the space of curves. This fact has been ignored in previous active contour literature; indeed previous active contours were always derived from the geometric $\mathbb{L}^2$-type (H^0) metric.[1] However, the work of Michor and Mumford (2006), Yezzi and Mennucci (2005a, 2005b) has shown that the geometric $\mathbb{L}^2$-type metric is not a true Riemannian metric, since the induced distance between curves is identically zero, and therefore $\mathbb{L}^2$ is unsuitable for *shape analysis*. Accordingly, Sundaramoorthi et al. (2005, 2006), Charpiat et al. (2005, 2007) have considered new metrics in the space of curves when deriving descent flows for active contours since it was shown by the authors that the usual $\mathbb{L}^2$ gradient descent has many undesirable properties. It was shown that the metric choice affects the path taken to minimize an energy, and that certain local minima of an energy can be avoided by designing an appropriate metric.

In particular, Sobolev metrics were considered. It was shown that gradient flows according to Sobolev metrics give smooth global flows, which avoid many local minima of energies that trap the usual $\mathbb{L}^2$ gradient flow. We should note that we are still minimizing the same energy, just with a different optimization procedure. Thereby, a critical point or a global minima, remains a critical point or global minima (resp.), these are properties of the energy itself and not the optimization procedure. The key difference is that the actual minimizing trajectory depends on the norm used to compute the gradient. We thereby, with Sobolev norms, obtain different gradients and as such different minimizing trajectories. In addition, it was shown that Sobolev metrics change the notion of "locality" in the space of curves and therefore make many local minimum, due to noise, in the space of curves vanish (Sundaramoorthi et al. 2008). In Sundaramoorthi et al. (2006, 2008), it was shown that Sobolev active contours move successively from coarse to finer scale motions, and therefore the method is suitable for tracking.

Applying Sobolev norms to variational problems has been done in areas other than active contours to gain many of the same advantages that are gained in active contour problems. For example, the book (Neuberger 1997) (see also references within) presents the theory of Sobolev gradients and applies it to various physical problems.

The Sobolev norm considered in much of the of the prior literature on Sobolev gradients is the usual Sobolev norm defined on a Banach (or Hilbert) space found in classical functional analysis texts, e.g. Rudin (1973). The key difference between those metrics and the ones we have considered (also considered by Charpiat et al. 2007) is that we have defined *geometrized* Sobolev norms; these are to be thought of as the metrics for a (yet to be completely studied) Riemannian manifold of curves, equivalent up to reparametrization. In addition to the geometrization of the standard Sobolev norm, which was also considered by Charpiat et al. (2007), we additionally proposed a non-standard geometrized Sobolev norm (see Definition 2.3), which we use exclusively in this paper. This non-standard Sobolev norm, in addition to yielding more computationally efficient flows (Sundaramoorthi et al. 2007) compared to the more standard version, also yields simple analytic solutions for the gradients of the energies that we consider in this paper.

The main purpose of Sundaramoorthi et al. (2005, 2006) was to show advantages of using Sobolev active contours over the traditional active contour based on the same energy. In contrast, in this paper we introduce *new* active contour energies that are quite useful for various segmentation tasks, but *cannot* be minimized with the traditional $\mathbb{L}^2$ active contour (nor other gradient descent for metrics proposed thus far), and the Sobolev active contour must be used. We show examples of these energies, which include simple geometric priors for active contours and new edge-based energies. These new energies fall into two categories: one in which the resulting traditional $\mathbb{L}^2$ flows are not stable, and another in which the traditional $\mathbb{L}^2$ gradient flow results in high order PDEs that are numerically difficult to implement using level set or particle based methods. We propose to use Sobolev active contours, which avoid both of these problems.

This paper is meant to illustrate that energies that result in $\mathbb{L}^2$ unstable or high order flows can still be considered for optimization with the Sobolev method (and these energies need not be discarded or adjusted). Experiments in this paper show the types of behaviors that can be obtained from the simple energies considered, and one can obtain good results on more complex images by combining these results with other energies.

[1] In this paper $\mathbb{L}^2$ will always refer to the standard *geometric* inner product (see Definition 2.2).

Before we proceed, we make brief remarks on other relevant energy minimizing approaches. The graph cut method (e.g., Kolmogorov and Boykov 2005) is often used to minimize geometric energies such as weighted length, flux of a vector field, and weighted area. This area of discrete optimization with techniques of this type continues to develop and more sophisticated energies are being shown to fall into the feasible category of optimizable energies. For example, curvature is being handled in certain cases (Schoenemann and Cremers 2007b), and simple prior shape information is now being included (Schoenemann and Cremers 2007a). The energies we use to exemplify the importance of Sobolev metrics in active contours are more general, and not all relevant energies can (yet) be handled by such graph cut types of approaches. For very general energies of importance, steepest descent methods are necessary, and therefore it is important to develop the right shape metrics for defining gradient descent flows as we show in this paper.

In addition to considering the Sobolev metric, Charpiat et al. (2005) (see also Mansouri et al. 2004) consider various different metrics resulting in 'coherent' gradient flows; indeed they construct flows that favor certain group motions such as affine motions. In the case of the affine group (others are analogous), the flow is formed by re-weighting the affine component of the traditional gradient higher and the component orthogonal (according to the $\mathbb{L}^2$ inner product) lower. These metrics are topologically equivalent to the traditional geometricized $\mathbb{L}^2$ metric in the sense that both metrics induce a distance between non-identical curves which is identically zero. While this does not preclude either of these metrics for use in shape optimization, it does render them pathological for applications to *shape analysis*. Moreover, for the class of energies that we wish to explore in this paper, the metrics based on group motions also suffer from the same problems as the traditional $\mathbb{L}^2$ metric; namely, these flows are either not stable or are high order PDEs and are difficult to implement numerically. The authors of Charpiat et al. (2005) also consider smoothing the standard $\mathbb{L}^2$ flow via a non-linear heat equation, which they term "Gaussian smoothing." This method was proposed mainly since such a method, although computationally intensive, is easily adapted to surfaces, unlike the Sobolev method. Although the Gaussian smoothing approach theoretically stabilizes some of the flows that we consider, when numerically implemented, we observe that instabilities arise due to the fact that numerically smoothing an ill-posed flow does not perfectly annihilate all the high frequency components in the flow causing the instabilities (see Sect. 6.1 for more details). This stresses the need for *analytical expressions* for the smoothed flow, which the Sobolev metrics that we consider provide, where the instabilities are perfectly annihilated. Still, for many other relevant problems, such flows considered by Charpiat et al. (2005) are shown to be highly effective (see also Eckstein et al. 2007).

2 Review of Sobolev Metrics and Gradients

Sobolev active contours were introduced in Sundaramoorthi et al. (2005, 2007). We now present an overview. Let M denote the set of immersed curves in $\mathbb{R}^d$ ($d \geq 2$), which is a differentiable manifold. For a curve $c \in M$, we denote by $T_c M$ the tangent space of M at c, which is isomorphic to the set of smooth perturbations of the form $h : S^1 \to \mathbb{R}^d$, where S^1 denotes the circle. We denote by $E : M \to \mathbb{R}$ an energy functional on M.

Definition 2.1 Let $E : M \to \mathbb{R}$.

If $c \in M$ and $h \in T_c M$, then the *variation of* E is $\mathrm{d}E(c) \cdot h = \frac{\mathrm{d}}{\mathrm{d}t} E(c+th)|_{t=0}$, where $(c+th)(\theta) := c(\theta) + th(\theta)$ and $\theta \in S^1$.

Assume $\langle \cdot, \cdot \rangle_c$ is an inner product on $T_c M$. The *gradient of* E is a vector field $\nabla E(c) \in T_c M$ that satisfies $\mathrm{d}E(c) \cdot h = \langle h, \nabla E(c) \rangle_c$ for all $h \in T_c M$.

One can interpret the gradient as the most efficient perturbation; that is, the gradient maximizes the change in energy per cost of perturbing the curve. The following proposition justifies the previous statement.

Proposition 2.1 *Let* $\| \cdot \|_c$ *be the norm induced from the inner product* $\langle \cdot, \cdot \rangle_c$ *on* $T_c M$. *Suppose* $\mathrm{d}E(c) \neq 0$, *and* $\nabla E(c)$ *exists*; *then the problem*

$$\sup_{\{h \in T_c M, \|h\|_c = 1\}} \mathrm{d}E(c) \cdot h = \sup_{\{k \in T_c M, k \neq 0\}} \frac{\mathrm{d}E(c) \cdot k}{\|k\|_c}$$

has a unique solution up to a multiplicative constant, $k = \nabla E(c) \in T_c M$, $h = k/\|k\|$.

The traditional inner product used to define active contours is the geometric $\mathbb{L}^2$-type inner product:

Definition 2.2 Let $c \in M$, L be the length of c, and $h, k \in T_c M$. We assume h and k are parameterized by the arclength parameter, s, of c. We define the $\mathbb{L}^2$ inner product by

$$\langle h, k \rangle_{\mathbb{L}^2, c} := \frac{1}{L} \int_c h(s) \cdot k(s) \, \mathrm{d}s.$$

Note that, contrary to the usual "parametric" $\mathbb{L}^2$ metric, we perform integration with respect to arclength-parameter. For this reason, the resulting space of curves is not a flat Euclidean space.

In Sundaramoorthi et al. (2007), we have explored the idea of changing the inner product above (i.e., changing the Riemannian metric on the space of curves) by looking at Sobolev-type inner products, which we review in the next section. Changing in this way the Riemannian metric associated with the space of curves regularizes the minimizing

flows associated with active contour energies without requiring the addition of regularization penalties in the original active contour energies. The change of metric does not affect the global minima of the energy, but it completely changes the notions of gradient and "*neighborhood of a curve*." As a result of the change of "locality," Sobolev active contours are much more robust to the local minima that strongly influence standard active contours, e.g., local minima due to noise (see Sundaramoorthi et al. 2008 for more details).

2.1 Sobolev Metrics on Closed Curves

We now present the definition of geometric Sobolev-type metrics used in this paper:

Definition 2.3 Let $c \in M$, L be the length of c, and $h, k \in T_c M$. We assume h and k are parameterized by the arc-length parameter, s, of c. Let $\lambda > 0$. Define

$$\overline{h} := \frac{1}{L}\int_c h(s)\,\mathrm{d}s,$$

and

$$\langle h, k\rangle_{\mathrm{Sobolev},c} := \overline{h}\cdot\overline{k} + \lambda L^{2n}\langle h^{(n)}, k^{(n)}\rangle_{\mathbb{L}^2,c},$$

where $h^{(n)}$ is the nth derivative of h with respect to arc-length.

Our choice of the definition of the Sobolev-type inner product above has two advantages over the usual definition of Sobolev inner products as the sum of all lower order derivatives: the corresponding formulas for gradient flows are much simpler, and the computational complexity to solve for the Sobolev metrics above is linear in the number of sample points of curve, whereas it is quadratic for the usual Sobolev definition. Moreover, the two Sobolev-type norms are topologically equivalent, and the corresponding gradient flows have the same qualitative behavior in many cases (see Sundaramoorthi et al. 2007, 2008).

We now review the details for calculating the Sobolev gradient in terms of the $\mathbb{L}^2$ metric. In this paper we are interested in first order Sobolev gradients ($n = 1$) to illustrate our concepts, and thus we give the formulas for computing the first order Sobolev gradient. It can be shown (Sundaramoorthi et al. 2007) that if E is an energy on the space of curves and $g = \nabla_{\mathrm{Sobolev}} E$ and $f = \nabla_{\mathbb{L}^2} E$, then

$$f(s) = \overline{f} - \lambda L^2 g''(s) \quad \text{where } s \in [0, L] \tag{1}$$

and we have periodic boundary conditions. This yields the solution

$$g(s) = g(0) + s g'(0) - \frac{1}{\lambda L^2}\int_0^s (s-\hat{s})(f(\hat{s}) - \overline{f})\,\mathrm{d}\hat{s}, \tag{2}$$

$$g'(s) = g'(0) - \frac{1}{\lambda L^2}\int_0^s (f(\hat{s}) - \overline{f})\,\mathrm{d}\hat{s}, \tag{3}$$

$$g'(0) = -\frac{1}{\lambda L^3}\int_0^L s(f(s) - \overline{f})\,\mathrm{d}s, \tag{4}$$

$$g(0) = \int_0^L f(s)K(s)\,\mathrm{d}s, \tag{5}$$

where

$$K(s) = \frac{1}{L}\left(1 + \frac{(s/L)^2 - (s/L) + 1/6}{2\lambda}\right), \quad s \in [0, L]. \tag{6}$$

We see that g and g' may also be written as a convolution:

$$g(s) = \int_c K(\hat{s} - s) f(\hat{s})\,\mathrm{d}\hat{s} =: (K * f)(s), \tag{7}$$

$$g'(s) = -(K' * f)(s) \tag{8}$$

and we have the important relation that will be quite useful for calculations below:

$$K''(s) = \frac{1}{\lambda L^2}\left(\frac{1}{L} - \delta(s)\right), \quad s \in [0, L). \tag{9}$$

It should be noted that for numerical purposes, one never uses the convolution formulas (7), (8), rather one uses the equivalent formulas (2), (3), which is linear in the sample points of the curve versus quadratic for (7), (8).

2.2 Sobolev Metrics on Open Curves with Fixed Endpoints

For some applications, e.g. using the elastic energy for curve interpolation (Horn 1983; Bruckstein and Netravali 1990; Mio et al. 2004) (see Sect. 3) or even segmentation tasks where curves hit the boundary of the image domain, it is necessary to look at metrics on open curves.

Definition 2.4 Let $c : [0, 1] \to \mathbb{R}^d$ such that $c(0) = p_0$, $c(1) = p_1$ where $p_0, p_1 \in \mathbb{R}^d$ are fixed. Let $h, k : [0, 1] \to \mathbb{R}^d$ be perturbations of c (i.e., $h(0) = h(1) = k(0) = k(1) = 0$), then we define the following inner products:

$$\langle h, k\rangle_{\mathbb{L}^2,c} := \frac{1}{L}\int_c h(s)\cdot k(s)\,\mathrm{d}s,$$

$$\langle h, k\rangle_{\mathrm{Sobolev},c} := L^{2n}\langle h^{(n)}, k^{(n)}\rangle_{\mathbb{L}^2,c},$$

where $h^{(n)}$ is the nth derivative of h with respect to arc-length.

Note that we no longer need the zero order term in the definition of Sobolev inner products since translations are no longer possible (with fixed endpoints). The computations become easier without the zero-order term, and moreover, the corresponding norms are equivalent to the norms that include the zero order term.

We now compute the Sobolev gradient in terms of the $\mathbb{L}^2$ gradient for order one ($n = 1$). Suppose E is an energy on c, and $g = \nabla_{\text{Sobolev}} E$ and $f = \nabla_{\mathbb{L}^2} E$, then

$$-L^2 g'' = f, \quad \text{with } g(0) = g(L) = 0.$$

This yields a solution of

$$g(s) = sg'(0) - \frac{1}{L^2}\int_0^s (s-\hat{s}) f(\hat{s})\,\mathrm{d}\hat{s}, \tag{10}$$

$$g'(s) = g'(0) + \frac{1}{L^2}\int_0^s f(\hat{s})\,\mathrm{d}\hat{s}, \tag{11}$$

$$g'(0) = \frac{1}{L^3}\int_0^L (L-\hat{s}) f(\hat{s})\,\mathrm{d}\hat{s}, \tag{12}$$

and a similar formula can be obtained for $g = \nabla_{\mathbb{L}^2} E$, in particular the solution is obtained in linear time. In terms of a kernel, we have that

$$g(s) = \hat{K}(f) = \int_0^L \hat{K}(s,\hat{s}) f(\hat{s})\,\mathrm{d}\hat{s}, \tag{13}$$

where

$$\hat{K}(s,\hat{s}) = \frac{1}{L}\begin{cases} \frac{\hat{s}}{L}(1-\frac{s}{L}), & 0 \le \hat{s} \le s, \\ \frac{s}{L}(1-\frac{\hat{s}}{L}), & s \le \hat{s} \le L, \end{cases} \tag{14}$$

and we have the relation

$$-L^2 \partial_{ss} \hat{K}(s,\hat{s}) = \delta(s-\hat{s}).$$

Notice that (13) is no longer a convolution as in the closed curve case, but more generally a symmetric linear operator.

3 Some Useful Energies Precluded by $\mathbb{L}^2$

In this section, we introduce three geometric "energies," which can be used as building blocks to produce a variety of other useful energies (to be described in subsequent sections). We then derive the $\mathbb{L}^2$ gradient and show that the gradient descent flow is either ill-posed or very difficult to implement numerically. We then derive the corresponding Sobolev gradient flows, and justify that they are well-posed and numerically feasible to implement. A rigorous proof of these results is quite difficult since these equations are *geometric, non-linear, non-local* PDE, and this is the subject of ongoing efforts (see also Proposition 4.1 in Sundaramoorthi et al. 2007). The property that ill-posed flows in one metric become well-posed in another metric shows that the ill-posedness is not solely due to the energy, but is also related to the metric chosen to define the gradient.

In this and subsequent sections, consider plane curves. We use the notation that if c is a plane curve, then

c_s = unit tangent vector to c,

c_{ss} = second derivative of c w.r.t. s,

$\mathcal{N}$ = unit inward normal of c,

$\kappa = c_{ss} \cdot \mathcal{N}$,

∂_s = derivative w.r.t. s.

The first "energy" that we introduce is the following generalization of average weighted length:

$$E(c) = \frac{1}{L}\int_c \phi(c(s))\,\mathrm{d}s = \overline{\phi}, \tag{15}$$

where $\phi : \mathbb{R}^2 \to \mathbb{R}^k$ where $k \ge 1$. The $\mathbb{L}^2$ gradient of this energy (see Appendix A.1) is

$$\nabla_{\mathbb{L}^2} E(c) = \mathcal{N}[\mathcal{N}^T (D\phi)^T - \kappa(\phi - \overline{\phi})^T], \tag{16}$$

where T denotes transpose, and D denotes derivative. Since $\phi - \overline{\phi}$ is not strictly positive, the gradient descent flow has a component that is reverse heat flow on roughly half of the contour, and therefore the $\mathbb{L}^2$ gradient descent is ill-posed. Note that the reverse heat component attempts to increase the length of certain portions of the contour. Since the ill-posedness of the $\mathbb{L}^2$ flow only arises from the length increasing effect, we expect the Sobolev gradient flow to be well-posed. This is because increasing the length of the contour is a well-posed process using the Sobolev gradient; indeed, the Sobolev gradient ascent for length is simply a rescaling of the contour (Sundaramoorthi et al. 2005). Computing the Sobolev gradient of (15) we have that (see Appendix A.1)

$$\nabla_{\text{Sobolev}} E(c) = -\frac{c - \overline{c}}{\lambda L^2}\overline{\phi}^T + K * (D\phi)^T + K' * (c_s \phi^T). \tag{17}$$

Notice that the component, $\mathcal{N}\overline{\phi}^T\kappa$, of the $\mathbb{L}^2$ gradient that caused the ill-posedness has been converted to the first term of the Sobolev gradient (17), which is a stable rescaling of the contour.

Next, we introduce a scaled version of the weighted area, given by the energy

$$E(c) = \frac{1}{L^2}\int_R \phi(x)\,\mathrm{d}A(x) = \frac{A_\phi}{L^2}, \tag{18}$$

where $\phi : \mathbb{R}^2 \to \mathbb{R}$, R is the region enclosed by c, and $\mathrm{d}A$ is the area measure in $\mathbb{R}^2$. Similar to the previous energy, the ill-posedness of the $\mathbb{L}^2$ gradient descent flow of (18) is due to the scale factor of L^{-2}, which causes a length increas-

ing component in the gradients, and is ill-posed with respect to $\mathbb{L}^2$. Indeed, calculating the gradient, we have

$$\nabla E(c) = \frac{L^2 \nabla A_\phi - 2A_\phi L \nabla L}{L^4} = \frac{A_\phi}{L^2}\left[\frac{\nabla A_\phi}{A_\phi} - 2\frac{\nabla L}{L}\right].$$

Therefore, we see that

$$\nabla_{\text{Sobolev}} E(c) = -\frac{A_\phi}{L^2}\left[L\frac{K * (\phi \mathcal{N})}{A_\phi} + 2\frac{c - \overline{c}}{\lambda L^2}\right], \tag{19}$$

which leads to a well-posed descent (and ascent).

Lastly, we introduce the following generalization of the elastic energy:

$$E(c) = L\int_c \phi(c(s))\kappa^2(s)\,\mathrm{d}s, \tag{20}$$

where $\phi : \mathbb{R}^2 \to \mathbb{R}$, and κ is the signed curvature of c. The factor of L multiplying the integral makes the energy scale-invariant when ϕ is a constant. Note that without the factor of L, one can make the elastic energy arbitrarily small by scaling a contour large enough. We will also consider the scale-varying elastic energy without the L for segmentation applications. These energies have been used in the past for the "curve completion" problem, which is a curve interpolation problem between two points (Horn 1983; Bruckstein and Netravali 1990). In Bruckstein and Netravali (1990), for the numerical implementation, a discrete version of the energy is minimized with a "shooting" method. One can show that the $\mathbb{L}^2$ gradient of (20) (see Appendix A.2) is

$$\begin{aligned}\nabla_{\mathbb{L}^2} E(c) = &-E c_{ss} + 2L^2 \partial_{ss}(\phi c_{ss}) \\ &+ 3L^2 \partial_s(\phi \kappa^2 c_s) + L^2 \kappa^2 \nabla\phi.\end{aligned} \tag{21}$$

We note the result of Polden (1996), which considers the $\mathbb{L}^2$ gradient descent flow of an energy similar to (20). The author considers the $\mathbb{L}^2$ gradient descent flow of the energy

$$E(c) = \int_c (\kappa^2(s) + \alpha)\,\mathrm{d}s,$$

where $\alpha > 0$. It is proven that an immersed/regular curve evolving under this fourth-order flow stays immersed/regular, and a solution exists for all time. In the case when ϕ is a constant, the flow (21) is similar to the flow that is considered in Polden (1996), except that α is time varying in (21). For numerical implementation, the fourth order flow (21) is difficult to implement with marker particle methods because of numerical artifacts arising from fourth order differences, and it is even more problematic (e.g. Droske and Rumpf 2004) to implement with level set methods because the flow is not known to have a maximum principle and because of numerical artifacts. This motivates us to consider the Sobolev gradient flow (see Appendix A.2):

$$\begin{aligned}\nabla_{\text{Sobolev}} E = &-\frac{E}{\lambda L^2}(\overline{c} - c) + \frac{2}{\lambda}(\overline{(\phi c_{ss})} - \phi c_{ss}) \\ &- 3L^2 K' * (\phi \kappa^2 c_s) + L^2 K * (\kappa^2 \nabla\phi).\end{aligned} \tag{22}$$

The Sobolev flow is second order, although it is an integral PDE. We can bypass the question about a maximum principle for this flow since the local terms have a maximum principle, and we perform extensions in the level set implementation for global terms.

4 Geometric Priors for Active Contours

In this section, we introduce some simple geometric shape priors for use in active contour segmentation. As these energies are formed from the energies presented in the previous section, they cannot be minimized with the usual $\mathbb{L}^2$ gradient descent.

4.1 Length and Smoothness Priors

In many active contour models, a curvature term, i.e., $\alpha\kappa\mathcal{N}$ (where $\alpha > 0$ is a weight), is added to a data-based curve evolution. The resulting flow will inherit regularizing properties such as smoothing the curve from the addition of this term. If the active contour model is based on minimizing an energy, then adding a curvature term is equivalent to adding a length penalty to the original energy, that is, if E_{data} is the original energy then the new energy being optimized (w.r.t. the traditional $\mathbb{L}^2$ metric) is

$$E(c) = E_{\text{data}}(c) + \alpha L(c). \tag{23}$$

This may be considered as a simple prior in which we assume that the length of the curve is to be shrunk. In general segmentation situations, this assumption may not be applicable. A more general energy incorporating length information, when such prior length information is known, is

$$E(c) = E_{\text{data}}(c) + \alpha(L(c) - L_0)^2, \tag{24}$$

in which it is assumed that length of the target curve is near L_0. Note that this prior allows for increasing or decreasing the length of the curve based on the current length of the curve and the value of L_0. The $\mathbb{L}^2$ gradient is

$$\nabla_{\mathbb{L}^2} E(c) = \nabla_{\mathbb{L}^2} E_{\text{data}}(c) - 2\alpha(L - L_0)\kappa\mathcal{N},$$

which leads to an unstable flow if $L - L_0 < 0$. The Sobolev gradient is

$$\nabla_{\text{Sobolev}} E(c) = \nabla_{\text{Sobolev}} E_{\text{data}}(c) + 2\alpha(L - L_0)\frac{c - \overline{c}}{\lambda L},$$

which is stable if the data term is stable.

One can also consider flows that preserve the length of curves rather than penalizing deviations from a target length. See Sapiro and Tannenbaum (1995) (and references within) for related flows where the length of the curve is preserved. To derive length preserving flows that minimize an energy, one can calculate the gradient flow and project it onto the subspace of length preserving perturbations. Traditionally, one has an $\mathbb{L}^2$ gradient, i.e., $\nabla_{\mathbb{L}^2} E(c)$, and an $\mathbb{L}^2$ projection is done onto the subspace of length preserving perturbations:

$$\pi_L(\nabla_{\mathbb{L}^2} E(c)) = \nabla_{\mathbb{L}^2} E(c) - \frac{\langle \nabla_{\mathbb{L}^2} E(c), \nabla_{\mathbb{L}^2} L(c)\rangle_{H^0}}{\langle \nabla_{\mathbb{L}^2} L(c), \nabla_{\mathbb{L}^2} L(c)\rangle_{H^0}} \nabla_{\mathbb{L}^2} L(c).$$

Note $\nabla_{\mathbb{L}^2} L(c) = c_{ss} = \kappa\mathcal{N}$. Thus,

$$\pi_L(\nabla_{\mathbb{L}^2} E(c)) = \nabla_{\mathbb{L}^2} E(c) - \frac{\langle \nabla_{\mathbb{L}^2} E(c), \kappa\mathcal{N}\rangle_{H^0}}{\int_c \kappa^2 \,\mathrm{d}s} \kappa\mathcal{N},$$

and the flow corresponding to the above will decrease the energy of interest while preserving the length of the curve. Depending on the sign of the inner product above, the flow may be ill-posed. For example, if we look at the simple Chan-Vese or Mumford-Shah $\mathbb{L}^2$ flows then the inner product may give a negative sign and result in backward heat flow. The Sobolev projection for preserving the length results in a well-posed process provided the original gradient descent is well-posed:

$$\pi_L(\nabla_{\text{Sobolev}} E(c)) = \nabla_{\text{Sobolev}} E(c) - \frac{\langle \nabla_{\text{Sobolev}} E(c), \frac{c-\overline{c}}{\lambda L^2}\rangle_{\text{Sobolev}}}{\frac{1}{\lambda L^4}\int_c |c-\overline{c}|^2 \,\mathrm{d}s} \frac{c-\overline{c}}{\lambda L^2}.$$

In active contour works, the goal of adding the usual length penalty may have been mainly for obtaining the regularizing properties of the resulting flow, even though the energy itself does not favor more regular curves. It is evident that the Sobolev length descent does not regularize the active contour since the flow is a rescaling of the curve. Thus, to introduce smoothness into the Sobolev active contour (and even the $\mathbb{L}^2$ active contour), we introduce the smoothness prior given by the energy,

$$E(c) = E_{\text{data}}(c) + \alpha L(c) \int_c \kappa^2(s) \,\mathrm{d}s. \tag{25}$$

The energy itself favors smoother contours, and we are not relying on the properties of a particular metric for regularity; it is inherent in the energy itself. The factor of L is for scale-invariance (unlike the length descent, this regularizer does not favor shrinking the length of the contour). Using the scale-varying and scale-invariant elastic energies as smoothness measures for active contours is mentioned but not implemented in Delingette (2001), Brook et al. (2005).

4.2 Centroid and Isoperimetric Priors

We now consider incorporating prior information on the centroid, length, and area of a curve into active contour segmentation. We consider the energy

$$E(c) = E_{\text{data}}(c) + \alpha\|\overline{c} - v\|^2 + \beta(L - L_0)^2 + \gamma(A - A_0)^2, \tag{26}$$

where $\alpha, \beta, \gamma \geq 0$ are weights, $\overline{c}$ is the centroid of the curve c, $v \in \mathbb{R}^2$ is the centroid known *a-priori* (see Sect. 6.3 for an example of how this may be obtained), L_0 and A_0 are the prior values for the length and area. If detailed information is not known about the length and area, then that part of the energy may be replaced by the energy

$$E(c) = E_{\text{data}}(c) + \alpha\|\overline{c} - v\|^2 + \beta(\rho(c) - \rho_0)^2, \tag{27}$$

where

$$\rho(c) = \frac{A(c)}{L^2(c)} \tag{28}$$

is the isoperimetric ratio, which is a geometric measure of the relative relation between the length and area of a curve. Note that ρ is scale-invariant. It is a well known fact that the isoperimetric ratio is maximized by circles, and the maximum ratio is $1/(4\pi)$. Thus, the prior ratio must be constrained so that $\rho_0 \leq 1/(4\pi)$. Note that a low (near zero) isoperimetric ratio can be obtained by a snake-like shape, and a high ratio implies a shape that looks close to a circle. The isoperimetric ratio is mentioned to be used as a smoothness measure in Delingette (2001), but this idea is not pursued.

Note that both the $\mathbb{L}^2$ gradient descents for the centroid constraint and the isoperimetric penalties are ill-posed. The isoperimetric ratio is a special case of (18) (when $\phi = 1$), and the constraint gives a gradient of $(\rho - \rho_0)\nabla\rho$, which gives an unstable $\mathbb{L}^2$ gradient descent flow when $\rho > \rho_0$. Note that the centroid is a special case of (15) (when $\phi : \mathbb{R}^2 \to \mathbb{R}^2$ is $\phi(x) = x$). The gradient of the centroid penalty is $\nabla(\overline{c})(\overline{c} - v)$, which gives an $\mathbb{L}^2$ gradient of

$$[(\overline{c} - v)\cdot\mathcal{N} - (c - \overline{c})\cdot(\overline{c} - v)\kappa]\mathcal{N}$$

using (16). The gradient descent is unstable when $(c - \overline{c})\cdot(\overline{c} - v) < 0$. The Sobolev gradient using (17) is

$$(\bar{c} - v) + K' * [c_s(c - \overline{c})\cdot(\overline{c} - v)].$$

One possible use for (26) and (27) is in tracking applications (see Sect. 6.3).

4.3 Shape Priors Based on Moments

In this section, we consider prior-based segmentation based on moments of prior shapes. In traditional prior-based image segmentation, one has a database of likely shapes, and a principal component analysis (PCA) or related statistics are computed on shapes in this database. In many papers on incorporating prior shape knowledge (e.g., Leventon et al. 2000; Tsai et al. 2001; Rousson and Paragios 2002), a "shape" is represented by its signed distance function and the PCA is done on aligned versions of these signed distance functions. An active contour energy is optimized on the subspace of "shapes" spanned by the first few modes of the PCA in order to segment an image incorporating the prior known set of likely shapes. Although PCA on signed distance functions is not well-founded since the space of signed distance functions is not a vector space, the method works well experimentally in many cases.

Other ways of incorporating prior shape information into the segmentation (e.g. Chen et al. 2002; Cremers and Soatto 2003; Raviv et al. 2004) is by considering an energy of the form

$$E(c,T) = E_{\text{image}}(c) + d(c, T \circ c_{\text{prior}}), \tag{29}$$

where d would ideally be a metric on curves and c_{prior} is the prior known shape. The parameter T is a pose transformation, which is used so that posed transformed versions of the shape of interest may also be segmented. In many works, d is a similarity score between the curves, and usually not a true metric since a good metric on the space of curves is not easy to define. To obtain c_{prior} one may compute the average with respect to d of shapes in a database, i.e., one can compute the shape that minimizes the sum squared distance d to shapes in the database. The advantage of this approach over the approach of Leventon et al. (2000), Tsai et al. (2001) is that the shape has more freedom to deform to shapes not represented in the database since this model does not restrict the shape to be a linear combination of principal components.

We look at the latter approach for prior-based segmentation and take d to be a similarity score between shape descriptors based on moments. Indeed, we consider the descriptors

$$\sigma_{n,m} = \frac{1}{L}\int_c \left(\frac{c_1(s)-\overline{c_1}}{\sigma_x}\right)^n \left(\frac{c_2(s)-\overline{c_2}}{\sigma_y}\right)^m \mathrm{d}s \tag{30}$$

$$= \frac{1}{L}\int_c \phi(c(s), \overline{c}, \sigma(c))\,\mathrm{d}s, \quad n,m \geq 3, \tag{31}$$

where $\sigma(c) = (\sigma_x(c), \sigma_y(c))$. The above are scale and translation invariant descriptors. Note that we can give similar definitions of moments that are rotation and affine invariant, but we look at the simple case of scale and translation invariance to demonstrate the principle. Therefore, the alignment of shapes in the prior database (as in Leventon et al. 2000; Tsai et al. 2001; Rousson and Paragios 2002) is no longer necessary. The explicit update of pose parameters that is necessary to obtain Euclidean and scale invariance of the prior based model (as in (29)) is also no longer necessary. One can do a PCA on shapes in the prior database, which are represented by up to order N of the moments in (30). Note of course that simple algebraic operations on moments do not guarantee that the resulting moment correspond to a shape in the considered class. One can then formulate an energy that penalizes deviations from the PCA to form d in (29). In the simplest case, we have that

$$d_{\text{prior}}(c) = \frac{1}{2}\sum_{n,m}^{n+m\leq N} w_{n,m}(\sigma_{n.m}(c) - \sigma_{n,m}(c_{\text{prior}}))^2, \tag{32}$$

where $\sigma_{n,m}(c_{\text{prior}})$ is the (n,m) moment of a shape in the database.

The $\mathbb{L}^2$ gradient descent of (32) is ill-posed as $\sigma_{n,m}$ it is a generalization of average weighted length (15). Therefore, we consider the Sobolev gradient (see Appendix A.3), which yields

$$\begin{aligned}\nabla_{\text{Sobolev}}\sigma_{n,m} = &-\left[\sigma_{n,m} + \frac{1}{2}\sigma\overline{\nabla_\sigma \phi}\right]\frac{c-\overline{c}}{\lambda L^2}\\ &+ K * \left[\nabla_x\phi + \frac{c-\overline{c}}{\sigma}\cdot\overline{\nabla_\sigma\phi}\right]\\ &+ K' * \left[\phi c_s - (c-\overline{c})\cdot\overline{\nabla_x\phi}c_s\right.\\ &\left.+ \frac{1}{2}\frac{(c-\overline{c})^2}{\sigma}\cdot\overline{\nabla_\sigma\phi}c_s\right] - \overline{\nabla_\sigma\phi},\end{aligned} \tag{33}$$

where $\nabla_x\phi$ denotes the derivative with respect to the first argument of ϕ and we have used the following notation:

$$\frac{c-\overline{c}}{\sigma} := \left(\frac{c_1-\overline{c_1}}{\sigma_x}, \frac{c_2-\overline{c_2}}{\sigma_y}\right),$$

$$\frac{c-\overline{c}}{\sigma}\overline{\nabla_\sigma\phi} := \left(\frac{c_1-\overline{c_1}}{\sigma_x}\overline{\nabla_{\sigma_x}\phi}, \frac{c_2-\overline{c_2}}{\sigma_y}\overline{\nabla_{\sigma_y}\phi}\right).$$

Note that a similar approach of prior-based image segmentation based on moments has been considered in Foulonneau et al. (2006), however, the moments are area-based moments:

$$\sigma_{n,m} = \frac{1}{A^{(n+m)/2+1}}\int_R (x-\overline{x})^m (y-\overline{y})^n\,\mathrm{d}x\,\mathrm{d}y,$$

where $\overline{x}$ and $\overline{y}$ are the standard coordinate area-based means. The authors go on to consider affine-invariant moments. A reason for using length-based moments over area-based moments is that the length-based moments are much more sensitive to and therefore better at discriminating protrusions

and fine-scale details of the curve. Therefore, it is easier to detect finer details of the prior curve with length-based moments with smaller order moments compared to the region-based case (see Sect. 6.4 for an experiment).

5 New Edge-Based Active Contour Models

The energy for the traditional edge-based technique (Caselles et al. 1995; Kichenassamy et al. 1995) (called geodesic active contours) is

$$E(c) = \int_c \phi(c(s))\,\mathrm{d}s, \tag{34}$$

where $\phi : \mathbb{R}^2 \to \mathbb{R}$ is chosen low near edges (a common example is $\phi = 1/(1 + \|\nabla(G * I)\|)$ where G is a Gaussian smoothing filter). There are several undesirable features of this model (even if a perfect edge-map ϕ is chosen). The energy has trivial (undesirable) minima and even minima that are not at the edges of the image (see for example Ma and Tagare 1999). This is in part due to the bias that the model has in preferring shorter length contours, which may not always be beneficial. Therefore, we propose new edge-based models.

5.1 Non-Shrinking Edge-Based Model

We propose to minimize the following non-length shrinking edge-based energy:

$$E(c) = \int_c \phi(c(s))(L^{-1} + \alpha L\kappa^2(s))\,\mathrm{d}s, \tag{35}$$

where $\alpha \geq 0$, which we claim alleviates some of the undesirable properties of (34). An energy, which is similar to (35) (except for the factor of L on the curvature term), is considered by Fua and Leclerc (1990), but a discrete version of the energy is used for implementation. The first term, $\frac{1}{L}\int_c \phi\,\mathrm{d}s$ (i.e., (35) when $\alpha = 0$), is the same as the energy used for the geodesic active contour model, but there is a scale factor of $1/L$. This removes the length shrinking effect of (34) in descent flows; in particular if there are no edges (ϕ is constant), then a descent flow will not shrink the contour. The $\mathbb{L}^2$ gradient of the first term (when $\alpha = 0$ in (35)) as noted in (16) is

$$-L(\phi - \overline{\phi})\kappa\mathcal{N} + L(\nabla\phi \cdot \mathcal{N})\mathcal{N},$$

which is zero when the contour is aligned on true edges of the image (note that this may not be the case with the geodesic active contour model). The flow is stable with respect to the Sobolev metric, but not with respect to $\mathbb{L}^2$.

Dividing the energy (34) by L, as in the first term of (35), loses regularizing effects of the original flow, and it is possible that the contour can become non-smooth from irrelevant noise. This observation is the reason for the second term of (35). The second term, $L\int_c \phi\kappa^2\,\mathrm{d}s$, is an image dependent version of the scale-invariant elastic energy. This term favors smooth contours, but smoothness is relaxed in the presence of edges, which are determined by ϕ. The factor of L makes the energy scale-invariant when ϕ is constant; therefore, a descent flow will not increase or decrease the length of the contour unless these behaviors make the curvature smaller or make the contour align along the edges. The reason for not considering this term alone is for the following. Suppose we are considering open curves with two endpoints fixed. Regardless of the ϕ that is chosen, the minimum of this term is always zero, and it is minimized by a straight line (the curvature is zero). For closed contours, we have observed in the numerical implementation that the contour sticks to isolated points where there is an edge of the image, and the converged contour is a straight line between these points (even if there is no edge along the line). Thus, the contour looks polygon-like. Even though the $\kappa = +\infty$ at vertices of polygons, this is not true numerically where κ is finite. Therefore, in a numerical implementation, the second term of (35) is not useful by itself.

5.2 Increasing Weighted Length

Instead of a non-shrinking edge-based model, if we have prior information that the length of the curve should increase, e.g., the initial curve is within the object of interest, then one may want to *maximize* the following energy:

$$E(c) = \int_c \phi(c(s))\,\mathrm{d}s - \alpha\int_c \kappa^2(s)\,\mathrm{d}s, \tag{36}$$

where $\alpha \geq 0$, and ϕ, contrary to the geodesic active contour model, is designed to be large near edges (one example is choosing $\phi = \|\nabla I\|$). The first term of the energy is a weighted length, and therefore this term favors increasing the length of the curve while stopping near edges. Considering only the first term ((36) when $\alpha = 0$), since the length of the curve is being increased, it is likely that when the curve has converged on a coarse scale, fine details due to noise become detected and the curve becomes rough, thereby further increasing length. Therefore, we add a regularizer, which is the second term of (36), to the weighted length. Note that we propose to use the scale-varying elastic energy, which in addition to regularity, gives an effect of increasing the length of the curve, which is beneficial based on the prior assumption.

The $\mathbb{L}^2$ gradient ascent of the weighted length term results in one term that is $-\phi\kappa\mathcal{N}$, which makes the length of the curve increase and is unstable. If $\alpha > 0$, then the $\mathbb{L}^2$ flow of (36) may become well-posed since this results in

Fig. 1 Flows increasing the length of the curve. *Left* to *right*: initial contour, after 100 and 400 iterations of smoothed backward heat flow (10 smoothing iterations), after 250 and 1000 iterations of smoothed backward heat flow (100 smoothing iterations), Sobolev gradient flow after 100 and 400 iterations (this is independent of λ). Notice that the Gaussian smoothed flow builds up irregularities numerically, and smoothing more helps delay the build up of the irregularities

higher order regularity terms, but the elastic energy has its own problems using the $\mathbb{L}^2$ gradient flow. Therefore, we use the Sobolev flow.

6 Experiments

In the following experiments, we use level set methods to implement the curve evolutions. The numerical implementation for Sobolev gradient flows follows what has been described in detail in Sundaramoorthi et al. (2007).

6.1 Stability of Length Increasing Flow

In this first experiment, we consider simple flows to increase the length of an initial curve. First, we consider the Gaussian smoothing approach of Charpiat et al. (2005), that is, we consider numerically implementing the flow $c_t = -S_\delta(c_{ss})$ where S_δ is a Gaussian smoothing operator. Note that since S_δ is the solution of the heat equation on the circle, one cannot obtain a closed form solution for S_δ as a convolution kernel as in the case of the Sobolev metric. Therefore, one is forced to numerically implement the smoothing process. In Fig. 1, we show that while theoretically the Gaussian smoothed flow is stable, the numerical implementation gives many irregularities, which are signs of instabilities. This is probably because the numerical smoothing does not annihilate exactly all of the high frequency components causing the instabilities of the original flow. On the other hand, the Sobolev gradient ascent is numerically stable as we have a closed form solution for its gradient (Fig. 1).

6.2 Regularity of Sobolev Active Contour

In this experiment, we show a case when the scale-invariant elastic regularity term (25) is more beneficial than the using the traditional length penalty (23). Note that the elastic regularizer does not generally have a length shrinking effect, but keeps the contour regular. This length shrinking effect may have a detrimental effect as shown in Fig. 2. Note that the length penalty restricts the curve from moving into the groves between the fingers. The elastic regularity term, on the other hand, has no such restriction, and makes the curve more smooth and rounded.

6.3 Tracking with Centroid/Isoperimetric Prior

In this experiment, we illustrate one possible application of the energy (27) in tracking a man through an occlusion. For the data-based term in (27), we use the Mumford-Shah energy (Mumford and Shah 1989). The prior information on the centroid and isoperimetric ratio can be obtained through a filtering process (indeed, we assume a constant acceleration model of both quantities). We use the tracking framework of Jackson et al. (2004) for the simulations in the last two rows of Fig. 3. In summary, the method of Jackson et al. (2004) (like many other tracking algorithms) consists of two steps: (1) a detection step, in which the curve is updated according to image data and (2) a prediction step, in which the curve is extrapolated forward according to predefined dynamics. The detection step involves a simultaneous segmentation and rigid registration (which we choose to be a simple translation) of three consecutive frames based on the energy (27). For the prediction, a constant acceleration model is assumed for the parameters of the rigid registration. The measurements that the estimator uses to estimate the contour and its registrations are the results of the detection step. A Kalman gain is used to determine if more weight is put on the measured contour versus the model prediction.

The top row shows the result using the framework of Jackson et al. (2004) without the use of prior centroid and isoperimetric information ($\alpha = \beta = 0$ in (27)) using the $\mathbb{L}^2$ descent. The middle row is the results of the experiment on the top row except that the descent of the data-based energy is done according to the Sobolev metric. Note that the Sobolev active contour improves the result, but is unable to pass through the occlusion. The bottom row incorporates prior information on the centroid and isoperimetric ratio ($\alpha = 50000$, $\beta = 100$ in (27)). Notice that the prior information on the centroid keeps the contour moving through the occlusion, while the isoperimetric ratio (and because Sobolev active contours favors coarse-scale motions such as translations) keeps the shape constrained.

6.4 Prior Shape Segmentation with Moments

We now show results of using simple shape priors based on moments for image segmentation. In the first experiment

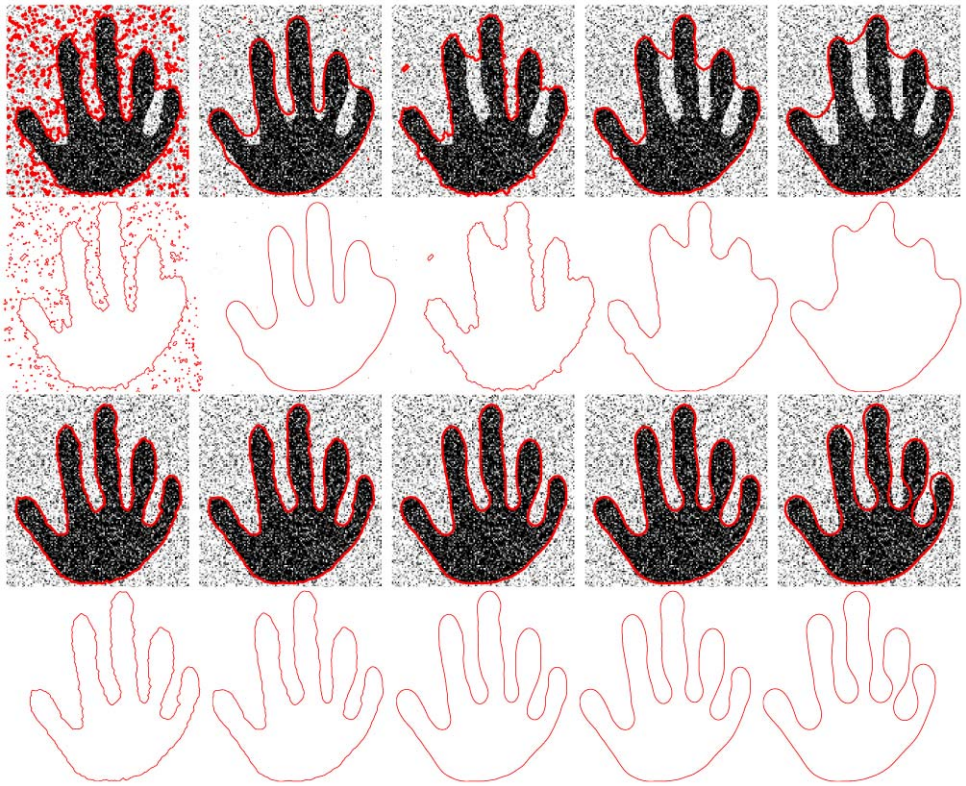

Fig. 2 $\mathbb{L}^2$ regularization (*top two rows*). *Left* to *right*: $\alpha = 1000$, $\alpha = 1000$ followed by curvature smoothing to remove the noise (least number of iterations to remove noise), $\alpha = 10000, 50000, 90000$. The image-based term is Chan-Vese. Sobolev elastic regularization (*bottom two rows*). *Left* to *right*: $\alpha = 0, 0.1, 5, 10, 25$. The *second* and *fourth row* show the same result as the *row* above them, but the image is removed for visibility

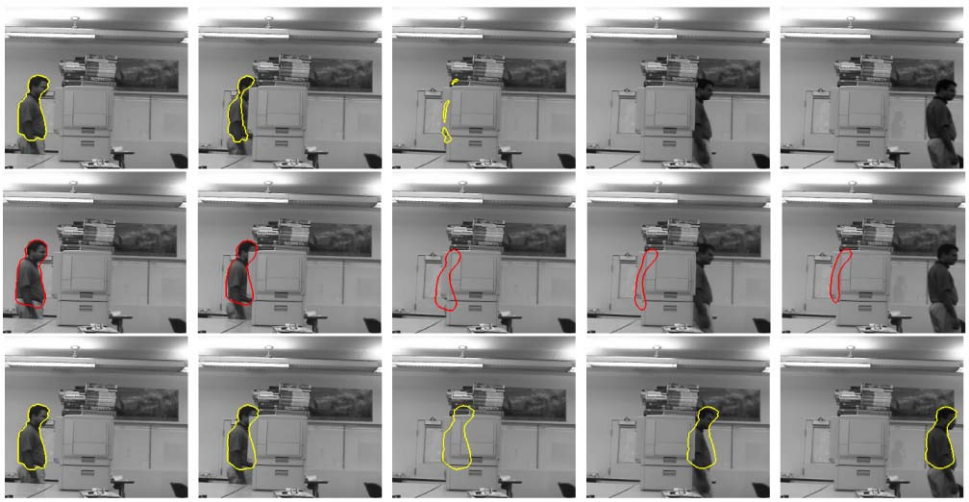

Fig. 3 Tracking a man through an occlusion. *Bottom row* shows the results of using a prediction (filtering) on the centroid and the isoperimetric ratio, and then penalizing deviations of the contour away from predicted parameters by (27) ($\alpha = 50000$, $\beta = 100$). The *top row* gives the result with no such penalty using usual $\mathbb{L}^2$ ($\alpha = \beta = 0$ in (27)), and the *middle row* is using Sobolev active contours with no prior ($\alpha = \beta = 0$ in (27))

(Fig. 4), we show the usefulness of incorporating a covariance prior for object tracking. In this experiment, we segment frame-wise using the energy

$$E(c) = E_{cv}(c) + \|\Sigma(c) - \Sigma(c_0)\|^2,$$

where E_{cv} is the Chan-Vese energy (Chan and Vese 2001), and

$$\Sigma(c) = \begin{pmatrix} \sigma_{2,0}(c) & \sigma_{1,1}(c) \\ \sigma_{1,1}(c) & \sigma_{0,2}(c) \end{pmatrix}, \quad \text{and}$$

$$\sigma_{ij}(c) = \frac{1}{L}\int_c (c_1(s) - \overline{c_1})^i (c_2(s) - \overline{c_2})^j \, \mathrm{d}s,$$

and c_0 is the initial curve in the first frame. Note that we are considering scale-varying variances since we would like to place a prior on the scale of the object. Figure 4 shows that without such a variance prior even with Sobolev active contours, the contour expands to the background since this portion of the background resembles the object more closely than the dark area. However, when adding a prior on the covariance obtained from the initial contour in the initial

Fig. 4 Tracking of a sea creature using a covariance prior from the initial frame. The *top row* shows the tracking using a simple Chan-Vese detection energy with Sobolev active contours. The *bottom row* shows the result when adding a simple covariance prior obtained from the initial frame, which can only be optimized with Sobolev active contours

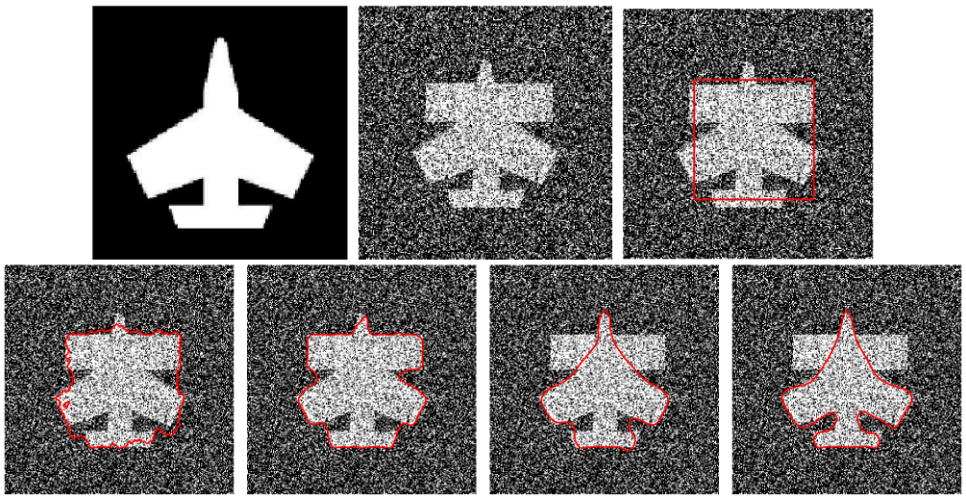

Fig. 5 Prior-based image segmentation based on moments. *Top row*: the first image is the prior shape from which 5th order moments are extracted, the second image is the image to be segmented, and the last image is the image to be segmented with the initial contour. *Bottom row*: final $\mathbb{L}^2$ active contour with no prior, Sobolev active contour with no prior, Sobolev active contour with area-based moment prior, and Sobolev active contour with length-based moment prior

frame, the curve is restricted from bleeding into the background.

In the experiment in Fig. 5, we perform a prior-based segmentation on a image that is both occluded and distorted by Gaussian noise (mean 0 and variance 0.6). We segment using the energy

$$E(c) = E_{cv}(c) + d_{\text{prior}}(c),$$

where d is defined in (32), and we use up to 5th order moments. The figure shows that without the moment-based priors, the segmentation captures the (unwanted) rectangle and cannot expand to capture the tail of the plane due to the high level of noise. The segmentation with area-based moments does much better and avoids the rectangular bar, but cannot expand in to capture the tail. The length-based moment prior segmentation avoids the rectangular bar and easily expands to capture the tail of the plane. This is because protrusions with large length and small area are much easier to capture with length-based moments. One could capture the tail with area-based moments, but one would need to use much higher moments, for example, in Foulonneau et al. (2006) the authors use around 40th order moments for their segmentation.

6.5 Edge Detection with Non-Shrinking Model

We first show an experiment (Fig. 6) to illustrate the behavior of the first term of the non-shrinking edge-based model (35). Because the standard edge-based energy prefers to shrink the curve in the absence of edge information, the corresponding flow (either in the H^0 or the Sobolev metrics) is not suitable for capturing concavities, where it is desirable to increase the length of the curve. Since the average value of the standard geodesic energy is not preferential to shrinking nor increasing the length of the curve and it is solely influenced by the edge information, this model has a better ability to capture concavities.

In this experiment, we demonstrate that the traditional edge-based geodesic active contour model has an arbitrary length shrinking effect that causes the contour to pass over some meaningful edges. We show that the non-shrinking edge-based model (35) can help correct this behavior. We use the edge-map, $1/(1+\phi)$, where

$$\phi(x) = \frac{1}{|B_r|}\int_{B_r(x)} (I(y) - \overline{I}_r(x))^2 \, \mathrm{d}A(y), \tag{37}$$

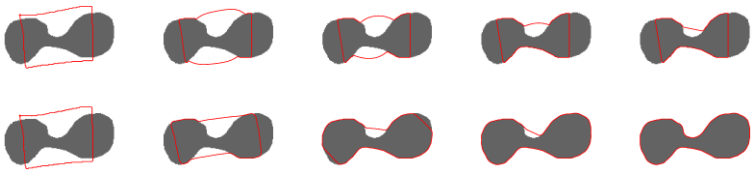

Fig. 6 Segmentation of concave object. Standard $\mathbb{L}^2$ geodesic active contour (*top*); the Sobolev active contour is similar, and using the first term of the non-shrinking model with Sobolev active contours (*bottom*)

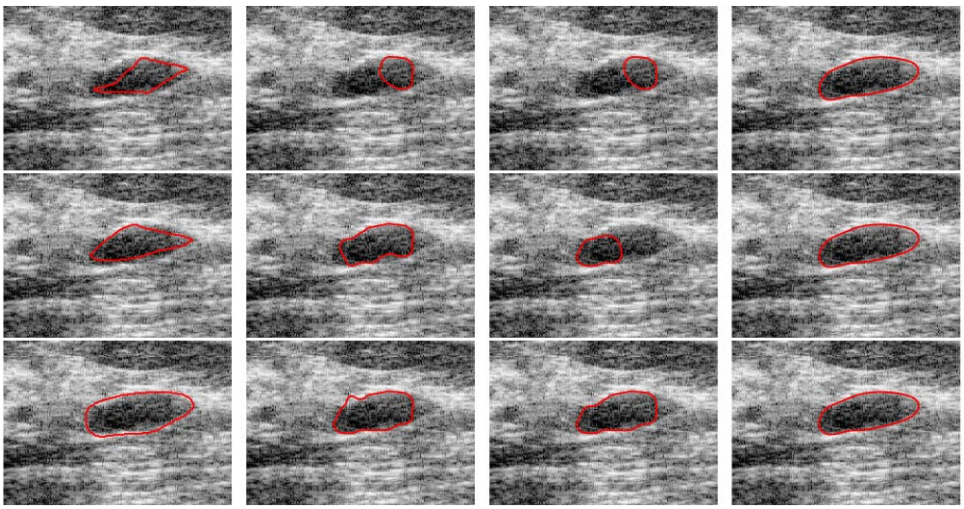

Fig. 7 Segmentation of cyst image with three different initializations (first image in *each row*). Converged results for the (34) and $\mathbb{L}^2$ active contour (second image), (34) with the Sobolev active contour (third image), and the energy (35) (last image)

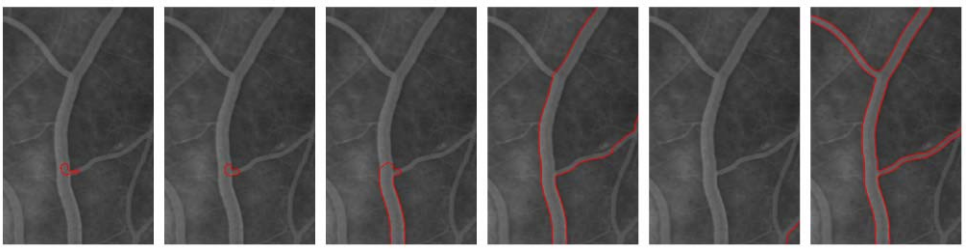

Fig. 8 *Left* to *right*: initial contour, minimizing (39) $\alpha = 0.2, 0.25, 0.4$ using $\mathbb{L}^2$, and increasing weighted (36) $\alpha = 0.1$ using Sobolev (all images show converged contour). The contour expands to enclose the entire image (fifth image)

$$\overline{I}_r(x) = \frac{1}{|B_r|}\int_{B_r(x)} I(y)\,\mathrm{d}A(y), \tag{38}$$

$B_r(x) = \{y \in \mathbb{R}^2 : \|y - x\| \le r\}$, and $|B_r|$ denotes the area of B_r.

In Fig. 7, we segment a cyst image using various initializations. Notice that the contour with the traditional edge-based energy (using the $\mathbb{L}^2$ or the Sobolev descents) consistently passes over the edge on the right side of the cyst. The non-shrinking model consistently captures the correct segmentation.

6.6 Edge Detection by Increasing Weighted Length

In this experiment, we apply the weighted length increasing energy (36) to vessel segmentation. We show the results of using the traditional edge-based technique with a balloon; that is, we show results of using the $\mathbb{L}^2$ gradient descent for the energy

$$E(c) = \int_c \phi(c(s))\,\mathrm{d}s - \alpha\int_R \phi\,\mathrm{d}A. \tag{39}$$

We use (37) as the edge-map for the weighted length increasing flow. The edge-map for (39) is $1/(1+\phi)$ where ϕ is given in (37).

In the case of vessel segmentation, it is beneficial to increase the length of the initial contour more so than area. Since a vessel is characterized as a long, thin structure, a balloon term will fail to capture the global geometry of the vessel. This is demonstrated in Fig. 8: a small weight on the balloon term results in the flow capturing local features close to the initial contour; larger weights on the balloon makes the contour balloon out to capture the entire image. Note the weighted length maximizing flow does not pass the walls of the vessel since that does not increase the *length* (although

it does increase area) of the contour, and is therefore able to capture the vessel.

7 Conclusion

We have demonstrated that the Sobolev gradient method allows one to consider active contour energies that were not considered in the past because the gradient method using the traditional metric cannot be used. In particular, we have given examples of energies that result in $\mathbb{L}^2$ gradients that are ill-posed or lead to high order PDEs (and hence numerically difficult to implement). These energies, as we have shown, result in Sobolev gradient flows that are both well-posed and numerically simple to implement. The experiments have shown potential uses for some energies introduced in segmentation and tracking applications.

Appendix A: Derivation of Sobolev Gradient Flows

Note that in this appendix, all Sobolev gradients are computed with respect to the first order ($n = 1$) Sobolev metric (2.3), and therefore, the expressions are in terms of the kernel, K, defined in (6). We recall the notation that if L is the length of a curve c and $f : [0, L] \to \mathbb{R}^d$ ($d \geq 2$) then

$$\overline{f} := \frac{1}{L}\int_c f(s)\,\mathrm{d}s.$$

Moreover, recall the notation presented in Sect. 3.

A.1 Average Weighted Length

Let

$$E(c) = \frac{1}{L}\int_c \phi(c(s))\,\mathrm{d}s,$$

where $\phi : \mathbb{R}^2 \to \mathbb{R}^k$ where $k \geq 1$. We now compute the $\mathbb{L}^2$ gradient for $k = 1$:

$$\begin{aligned}\nabla_{\mathbb{L}^2}E(c) &= -\frac{\nabla_{\mathbb{L}^2}L}{L}E(c) + \frac{1}{L}\nabla_{\mathbb{L}^2}(LE(c))\\ &= E\kappa\mathcal{N} + (\nabla\phi\cdot\mathcal{N})\mathcal{N} - \phi\kappa\mathcal{N}\\ &= (\nabla\phi\cdot\mathcal{N})\mathcal{N} - (\phi - E)\kappa\mathcal{N}. \qquad (40)\end{aligned}$$

For the general case of k, we find

$$\nabla_{\mathbb{L}^2}E(c) = \mathcal{N}[\mathcal{N}^T(D\phi)^T - \kappa(\phi - E)^T],$$

where T denotes transpose. We now compute the Sobolev gradient for $k = 1$:

$$\nabla_{\text{Sobolev}}E(c) = -\frac{\nabla_{\text{Sobolev}}L}{L}E(c) + \frac{1}{L}\nabla_{\text{Sobolev}}(LE(c))$$

$$\begin{aligned}&= -E\frac{c-\overline{c}}{\lambda L^2} + K * \nabla\phi + K' * (\phi c_s) \qquad (41)\\ &= -E\frac{c-\overline{c}}{\lambda L^2} + \frac{\phi c - \overline{\phi c}}{\lambda L^2}\\ &\quad - (\phi_s c) * K' + \nabla\phi * K, \qquad (42)\end{aligned}$$

where $\phi_s = \mathrm{d}/\mathrm{d}s\phi(c(s))$. For the general case of k, we find

$$\begin{aligned}\nabla_{\text{Sobolev}}E(c) &= -\frac{c-\overline{c}}{\lambda L^2}E^T + K * (D\phi)^T + K' * (c_s\phi^T)\\ &= -\frac{c-\overline{c}}{\lambda L^2}E^T + \frac{c\phi^T - \overline{c\phi^T}}{\lambda L^2}\\ &\quad - (c\phi_s^T) * K' + (D\phi)^T * K.\end{aligned}$$

A.2 Scale-Invariant-Type Elastic Energy

Let

$$E(c) = L\int_c \phi(c(s))\kappa^2(s)\,\mathrm{d}s.$$

We denote $C : S^1 \times [0, 1] \to \mathbb{R}^d$ ($C(p, t) \in \mathbb{R}^d$) to be a time varying family of curves, and we will write $E(t) := E(C(\cdot, t))$. First note that

$$C_{sst} = C_{tss} - (C_{tss}\cdot C_s + C_{ts}\cdot C_{ss})C_s - 2(C_{ts}\cdot C_s)C_{ss},$$

and since $C_s \cdot C_{ss} = 0$, we have that

$$\begin{aligned}\frac{\partial}{\partial t}(C_{ss}\cdot C_{ss}) &= 2C_{sst}\cdot C_{ss}2(C_{tss}\cdot C_{ss})\\ &\quad - 4(C_{ts}\cdot C_s)(C_{ss}\cdot C_{ss}). \qquad (43)\end{aligned}$$

Next we find that

$$\begin{aligned}\frac{\partial}{\partial t}(\phi(C)|C_p|) &= \nabla\phi\cdot C_t|C_p| + \phi\frac{C_{tp}\cdot C_p}{|C_p|}\\ &= (C_t\cdot\nabla\phi + \phi(C_{ts}\cdot C_s))|C_p|. \qquad (44)\end{aligned}$$

Now,

$$\begin{aligned}E'(t) &= \frac{\mathrm{d}}{\mathrm{d}t}\left(L\int_0^1 \phi(C)(C_{ss}\cdot C_{ss})|C_p|\,\mathrm{d}p\right)\\ &= \frac{E}{L}L_t + L\int_0^1 \frac{\partial}{\partial t}(\phi(C)|C_p|)C_{ss}\cdot C_{ss}\,\mathrm{d}p\\ &\quad + L\int_C \phi(C)\frac{\partial}{\partial t}(C_{ss}\cdot C_{ss})\,\mathrm{d}s.\end{aligned}$$

By substituting (43) and (44) into the last expression above, we have that

$$E'(t) = \int_C C_t\cdot\left(-\frac{E}{L}C_{ss} + L(C_{ss}\cdot C_{ss})\nabla\phi\right)\mathrm{d}s$$

$$+ L\int_C (2\phi(C_{tss}\cdot C_{ss}) - 3\phi(C_{ts}\cdot C_s)(C_{ss}\cdot C_{ss}))\,\mathrm{d}s.$$

Integrating by parts, we find that

$$E'(t) = \frac{1}{L}\int_C C_t\cdot(-EC_{ss} + 2L^2\partial_{ss}(\phi C_{ss}) + 3L^2\partial_s(\phi(C_{ss}\cdot C_{ss})C_s) + L^2(C_{ss}\cdot C_{ss})\nabla\phi)\,\mathrm{d}s.$$

Hence,

$$\nabla_{\mathbb{L}^2}E(c) = -Ec_{ss} + 2L^2\partial_{ss}(\phi c_{ss}) + 3L^2\partial_s(\phi(c_{ss}\cdot c_{ss})c_s) + L^2(c_{ss}\cdot c_{ss})\nabla\phi. \tag{45}$$

This form will be useful in computing the Sobolev gradient, but we simplify the expression (45) to understand the $\mathbb{L}^2$ flow in the planar case:

$$\partial_{ss}(\phi c_{ss}) = \partial_{ss}(\phi\kappa\mathcal{N})(\phi_{ss}\kappa + 2\phi_s\kappa_s + \phi\kappa_{ss} - \phi\kappa^3)\mathcal{N} - (2\phi_s\kappa^2 + 3\phi\kappa\kappa_s)c_s;$$

also,

$$\partial_s(\phi(c_{ss}\cdot c_{ss})c_s) = \partial_s(\phi\kappa^2 c_s) = (\phi_s\kappa^2 + 2\phi\kappa\kappa_s)c_s + \phi\kappa^3\mathcal{N}.$$

Therefore,

$$2\partial_{ss}(\phi c_{ss}) + 3\partial_s(\phi(c_{ss}\cdot c_{ss})c_s) = (2\phi_{ss}\kappa + 4\phi_s\kappa_s + 2\phi\kappa_{ss} + \phi\kappa^3)\mathcal{N} - \phi_s\kappa^2 c_s,$$

and finally,

$$\nabla_{\mathbb{L}^2}E(c) = L^2\Big(-\frac{E}{L^2}\kappa + 2\phi_{ss}\kappa + 4\phi_s\kappa_s + 2\phi\kappa_{ss} + \phi\kappa^3 + \kappa^2\nabla\phi\cdot\mathcal{N}\Big)\mathcal{N}. \tag{46}$$

Computing the Sobolev gradient from (45), we have that

$$\nabla_{\text{Sobolev}}E = K*\nabla_{\mathbb{L}^2}E = -EK''*c + 2L^2K''*(\phi c_{ss}) - 3L^2K'*(\phi(c_{ss}\cdot c_{ss})c_s) + L^2K*((c_{ss}\cdot c_{ss})\nabla\phi).$$

Hence,

$$\nabla_{\text{Sobolev}}E = -\frac{E}{\lambda L^2}(\overline{c}-c) + \frac{2}{\lambda}(\overline{(\phi c_{ss})} - \phi c_{ss}) - 3L^2K'*(\phi\kappa^2 c_s) + L^2K*(\kappa^2\nabla\phi). \tag{47}$$

A.3 Moments

We calculate the gradients of the moments defined by

$$\sigma_{n,m} = \frac{1}{L}\int_c\Big(\frac{c_1(s)-\overline{c_1}}{\sigma_x}\Big)^n\Big(\frac{c_2(s)-\overline{c_2}}{\sigma_y}\Big)^m\mathrm{d}s = \frac{1}{L}\int_c\phi(c(s),\overline{c},\sigma_x,\sigma_y)\,\mathrm{d}s$$

where $n, m \geq 3$ and

$$\sigma_x^2 = \frac{1}{L}\int_c(c_1(s)-\overline{c_1})^2\,\mathrm{d}s, \quad \text{and}$$

$$\sigma_y^2 = \frac{1}{L}\int_c(c_2(s)-\overline{c_2})^2\,\mathrm{d}s.$$

We will denote ∇_x, D_{σ_x}, D_{σ_y} to be the derivative w.r.t. the first, third and fourth argument of ϕ. Then

$$\begin{aligned}\frac{\mathrm{d}}{\mathrm{d}t}\sigma_{n,m}(C(t)) &= \frac{1}{L}\int_C C_t\cdot\big[EC_{ss} + \nabla_x\phi - (\phi C_s)_s - \nabla_{\mathbb{L}^2}(\overline{C})\overline{\nabla_x\phi}\big]\,\mathrm{d}s \\ &\quad + \frac{1}{L}\int_C\Big(D_{\sigma_x}\phi\cdot\frac{\mathrm{d}}{\mathrm{d}t}\sigma_x + D_{\sigma_y}\phi\cdot\frac{\mathrm{d}}{\mathrm{d}t}\sigma_y\Big)\,\mathrm{d}s \\ &= \frac{1}{L}\int_C C_t\cdot\big[EC_{ss} + \nabla_x\phi - (\phi C_s)_s - \nabla_{\mathbb{L}^2}(\overline{C})\overline{\nabla_x\phi}\big]\,\mathrm{d}s \\ &\quad + \frac{1}{L}\int_C C_t\cdot\big[(\overline{D_{\sigma_x}\phi})\nabla_{\mathbb{L}^2}\sigma_x\big]\,\mathrm{d}s \\ &\quad + \frac{1}{L}\int_C C_t\cdot\big[(\overline{D_{\sigma_y}\phi})\nabla_{\mathbb{L}^2}\sigma_y)\big]\,\mathrm{d}s \\ &= \frac{1}{L}\int_C C_t\cdot\big[EC_{ss} + \nabla_x\phi - (\phi C_s)_s - \nabla_{\mathbb{L}^2}(\overline{C})\overline{\nabla_x\phi} \\ &\quad + \nabla_{\mathbb{L}^2}\sigma_x\overline{D_{\sigma_x}\phi} + \nabla_{\mathbb{L}^2}\sigma_y\overline{D_{\sigma_y}\phi}\big]\,\mathrm{d}s,\end{aligned}$$

and therefore,

$$\nabla_{\text{Sobolev}}\sigma_{n,m} = -E\frac{c-\overline{c}}{\lambda L^2} + K*\nabla_x\phi + K'*(\phi c_s) - \nabla_{\text{Sobolev}}(\overline{c})\overline{\nabla_x\phi} + \nabla_{\text{Sobolev}}\sigma_x\overline{D_{\sigma_x}\phi} + \nabla_{\text{Sobolev}}\sigma_y\overline{D_{\sigma_y}\phi}.$$

Note that

$$\nabla_{\text{Sobolev}}\sigma_x = \frac{1}{2\sigma_x}\Big[-\frac{c-\overline{c}}{\lambda L^2}\sigma_x^2 + 2K*(c_1-\overline{c_1}) + K'*(c_s(c_1-\overline{c_1})^2)\Big],$$

and so setting $\sigma = (\sigma_x, \sigma_y)$ and $\nabla_\sigma \phi = (D_{\sigma_x}\phi, D_{\sigma_y}\phi)$, we have

$$\begin{aligned}
&\nabla_{\text{Sobolev}\sigma}\overline{\nabla_\sigma \phi} \\
&\quad = -\frac{c-\overline{c}}{2\lambda L^2}(\sigma \cdot \overline{\nabla_\sigma \phi}) + K * \left[\left(\frac{c_1-\overline{c_1}}{\sigma_x}, \frac{c_2-\overline{c_2}}{\sigma_y}\right)\cdot \overline{\nabla_\sigma \phi}\right] \\
&\qquad + \frac{1}{2}K' * \left[c_s\left(\frac{(c_1-\overline{c_1})^2}{\sigma_x}, \frac{(c_2-\overline{c_2})^2}{\sigma_y}\right)\cdot \overline{\nabla_\sigma \phi}\right] \\
&\quad = -\frac{c-\overline{c}}{2\lambda L^2}(\sigma \cdot \overline{\nabla_\sigma \phi}) + K * \left[\frac{c-\overline{c}}{\sigma}\overline{\nabla_\sigma \phi}\right] \\
&\qquad + \frac{1}{2}K' * \left[c_s\frac{(c-\overline{c})^2}{\sigma}\cdot \overline{\nabla_\sigma \phi}\right],
\end{aligned}$$

where

$$\begin{aligned}
&\frac{c-\overline{c}}{\sigma} := \left(\frac{c_1-\overline{c_1}}{\sigma_x}, \frac{c_2-\overline{c_2}}{\sigma_y}\right), \\
&\frac{c-\overline{c}}{\sigma}\overline{\nabla_\sigma \phi} := \left(\frac{c_1-\overline{c_1}}{\sigma_x}\overline{D_{\sigma_x}\phi}, \frac{c_2-\overline{c_2}}{\sigma_y}\overline{D_{\sigma_y}\phi}\right).
\end{aligned}$$

Therefore,

$$\begin{aligned}
&\nabla_{\text{Sobolev}}\sigma_{n,m} \\
&\quad = -E\frac{c-\overline{c}}{\lambda L^2} + K * \nabla_x \phi + K' * (\phi c_s) \\
&\qquad - \overline{\nabla_x \phi} - K' * [c_s(c-\overline{c})\overline{\nabla_x \phi}] \\
&\qquad - \frac{c-\overline{c}}{2\lambda L^2}(\sigma \cdot \overline{\nabla_\sigma \phi}) + K * \left[\frac{c-\overline{c}}{\sigma}\overline{\nabla_\sigma \phi}\right] \\
&\qquad + \frac{1}{2}K' * \left[c_s\frac{(c-\overline{c})^2}{\sigma}\cdot \overline{\nabla_\sigma \phi}\right] \\
&\quad = -\left[\sigma_{n,m} + \frac{1}{2}\sigma \cdot \overline{\nabla_\sigma \phi}\right]\frac{c-\overline{c}}{\lambda L^2} \\
&\qquad + K * \left[\nabla_x \phi + \frac{c-\overline{c}}{\sigma}\overline{\nabla_\sigma \phi}\right] \\
&\qquad + K' * \left[\phi c_s - [(c-\overline{c})\cdot \overline{\nabla_x \phi}]c_s\right. \\
&\qquad \left. + \frac{1}{2}\left[\frac{(c-\overline{c})^2}{\sigma}\cdot \overline{\nabla_\sigma \phi}\right]c_s\right] - \overline{\nabla_\sigma \phi}.
\end{aligned}$$

Note that

$$\phi(x, y, \sigma_x, \sigma_y) = \left(\frac{x-\overline{x}}{\sigma_x}\right)^n \left(\frac{y-\overline{y}}{\sigma_y}\right)^m,$$

and

$$\nabla_x \phi = \begin{cases} (n[(x-\overline{x})\sigma_x^{-1}]^{n-1}[(y-\overline{y})\sigma_y^{-1}]^m, & \\ m[(x-\overline{x})\sigma_x^{-1}]^n[(y-\overline{y})\sigma_y^{-1}]^{m-1}), & n, m \neq 0, \\ (0, m[(y-\overline{y})\sigma_y^{-1}]^{m-1}), & n = 0, \\ (n[(x-\overline{x})\sigma_x^{-1}]^{n-1}, 0), & m = 0 \end{cases}$$

and

$$\nabla_\sigma \phi = -\begin{cases} (n\sigma_x^{-1}[(x-\overline{x})\sigma_x^{-1}]^n[(y-\overline{y})\sigma_y^{-1}]^m, & \\ m\sigma_y^{-1}[(x-\overline{x})\sigma_x^{-1}]^n[(y-\overline{y})\sigma_y^{-1}]^m), & \\ \quad n, m \neq 0, & \\ (0, m\sigma_y^{-1}[(y-\overline{y})\sigma_y^{-1}]^m), & n = 0, \\ (n\sigma_x^{-1}[(x-\overline{x})\sigma_x^{-1}]^m, 0), & n = 0. \end{cases}$$

References

Boykov, Y., & Jolly, M.-P. (2001). Interactive graph cuts for optimal boundary and region segmentation of objects in N–D images. In *ICCV* (pp. 105–112).

Brook, A., Bruckstein, A. M., & Kimmel, R. (2005). On similarity-invariant fairness measures. In *Scale-Space* (pp. 456–467).

Bruckstein, A. M., & Netravali, A. N. (1990). On minimal energy trajectories. *Computer Vision, Graphics, and Image Processing*, *49*(3), 283–296.

Caselles, V., Catte, F., Coll, T., & Dibos, F. (1993). A geometric model for edge detection. *Numerische Mathematik*, *66*, 1–31.

Caselles, V., Kimmel, R., & Sapiro, G. (1995). Geodesic active contours. In *Proceedings of the IEEE int. conf. on computer vision* (pp. 694–699). Cambridge, MA, USA.

Chan, T., & Vese, L. (2001). Active contours without edges. *IEEE Transactions on Image Processing*, *10*(2), 266–277.

Charpiat, G., Keriven, R., Pons, J., & Faugeras, O. (2005). Designing spatially coherent minimizing flows for variational problems based on active contours. In *ICCV*.

Charpiat, G., Maurel, P., Keriven, R., Pons, J.-P., & Faugeras, O. D. (2007). Generalized gradients: priors on minimization flows. *International Journal of Computer Vision*, *73*(3), 325–344.

Chen, Y., Tagare, H., Thiruvenkadam, S., Huang, F., Wilson, D., Gopinath, K., Briggs, R., & Geiser, E. (2002). Using prior shapes in geometric active contours in a variational framework. *International Journal of Computer Vision*, *50*(3), 315–328.

Cohen, L. D., & Kimmel, R. (1996). Global minimum for active contour models: a minimal path approach. In *CVPR* (pp. 666–673).

Cremers, D., & Schnörr, C. (2001). Diffusion-snakes: combining statistical shape knowledge and image information in a variational framework. In *Proc. IEEE workshop on variational, geometric, level set methods in computer vision* (pp. 137–144).

Cremers, D., & Soatto, S. (2003). A pseudo distance for shape priors in level set segmentation. In *IEEE int. workshop on variational, geometric and level set methods* (pp. 169–176).

Delingette, H. (2001). On smoothness measures of active contours and surfaces. In *VLSM '01: Proceedings of the IEEE workshop on variational and level set methods (VLSM'01)* (p. 43). Washington, DC, USA.

Droske, M., & Rumpf, M. (2004). A level set formulation for the willmore flow. *Interfaces and Boundaries*, *6*(3), 361–378.

Eckstein, I., Pons, J., Tong, Y., Kuo, C., & Desbrun, M. (2007). Generalized surface flows for mesh processing. In *Symposium on geometry processing* (pp. 183–192).

Foulonneau, A., Charbonnier, P., & Heitz, F. (2006). Affine-invariant geometric shape priors for region-based active contours. *IEEE Transactions on Pattern Analysis and Machine Intelligence*, *28*(8), 1352–1357.

Fua, P., & Leclerc, Y. G. (1990). Model driven edge detection. *Machine Vision and Applications*, *3*(1), 45–56.

Guyader, C. L., & Vese, L. (2007). *Self-repelling snakes for topology segmentation models* (Technical Report). UCLA.

Horn, B. K. P. (1983). The curve of least energy. *ACM Transactions on Mathematical Software*, *9*(4), 441–460.

Jackson, J., Yezzi, A., & Soatto, S. (2004). Tracking deformable moving objects under severe occulsions. In *IEEE conference on decision and control*.

Kass, M., Witkin, A., & Terzopoulos, D. (1987). Snakes: active contour models. *International Journal of Computer Vision*, *1*, 321–331.

Kichenassamy, S., Kumar, A., Olver, P., Tannenbaum, A., & Yezzi, A. (1995). Gradient flows and geometric active contour models. In *Proceedings of the IEEE int. conf. on computer vision* (pp. 810–815).

Kim, J., Fisher, J., Yezzi, A., Cetin, M., & Willsky, A. (2002). Nonparametric methods for image processing using information theory and curve evolution. In *IEEE international conference on image processing* (Vol. 3, pp. 797–800).

Kolmogorov, V., & Boykov, Y. (2005). What metrics can be approximated by geo-cuts, or global optimization of length/area and flux. In *ICCV* (pp. 564–571).

Leventon, M., Grimson, E., & Faugeras, O. (2000). Statistical shape influence in geodesic active contours. In *IEEE conf. on comp. vision and patt. recog.* (Vol. 1, pp. 316–323).

Ma, T., & Tagare, H. (1999). Consistency and stability of active contours with Euclidean and non-Euclidean arc lengths. *IEEE Transactions on Image Processing*, *8*(11), 1549–1559.

Malladi, R., Sethian, J., & Vemuri, B. (1995). Shape modeling with front propagation: a level set approach. *IEEE Transactions on Pattern Analysis and Machine Intelligence*, *17*(2), 158–175.

Mansouri, A.-R., Mukherjee, D. P., & Acton, S. T. (2004). Constraining active contour evolution via Lie Groups of transformation. *IEEE Transactions on Image Processing*, *13*(6), 853–863.

Michor, P. W., & Mumford, D. (2006). Riemannian geometries of space of plane curves. *Journal of the European Mathematical Society*, *8*, 1–48.

Mio, W., Srivastava, A., & Klassen, E. (2004). Interpolations with elasticae in Euclidean spaces. *Quaterly of Applied Mathematics*, *LXII*(3), 359–378.

Mumford, D., & Shah, J. (1985). Boundary detection by minimizing functionals. In *Proc. IEEE conf. computer vision pattern recognition*.

Mumford, D., & Shah, J. (1989). Optimal approximations by piecewise smooth functions and associated variational problems. *Communications on Pure and Applied Mathematics*, *42*, 577–685.

Nain, D., Yezzi, A. J., & Turk, G. (2004). Vessel segmentation using a shape driven flow. In *MICCAI (1)* (pp. 51–59).

Neuberger, J. W. (1997). *Sobolev gradients and differential equations*. *Lecture notes in mathematics*, *Vol. 1670*. Berlin: Springer.

Paragios, N., & Deriche, R. (2000). Geodesic active contours and level sets for the detection and tracking of moving objects. *IEEE Transactions on Pattern Analysis and Machine Intelligence*, *22*, 266–280.

Paragios, N., & Deriche, R. (2002). Geodesic active regions and level set methods for supervised texture segmentation. *International Journal of Computer Vision*, *46*(3), 223.

Polden, A. (1996). *Curves and surfaces of least total curvature and fourth-order flows*. Ph.D. thesis, Mathematisches Institut Universitat Tubingen, Germany.

Raviv, T. R., Kiryati, N., & Sochen, N. (2004). Unlevel-set: geometry and prior-based segmentation. In *Proc. European conf. on computer vision*.

Rochery, M., Jermyn, I., & Zerubia, J. (2003). Higher order active contours and their application to the detection of line networks in satellite imagery. In *IEEE Workshop on VLSM*.

Ronfard, R. (1994). Region based strategies for active contour models. *International Journal of Computer Vision*, *13*(2), 229–251.

Rousson, M., & Paragios, N. (2002). Shape priors for level set representations. In *Proc. European conf. computer vision* (Vol. 2, pp. 78–93).

Rudin, W. (1973). *Functional analysis*. New York: McGraw-Hill.

Sapiro, G., & Tannenbaum, A. (1995). Area and length preserving geometric invariant scale-spaces. *IEEE Transactions on Pattern Analysis and Machine Intelligence*, *17*(1), 67–72.

Schoenemann, T., & Cremers, D. (2007a). Globally optimal image segmentation with an elastic shape prior. In *IEEE international conference on computer vision (ICCV)*. Rio de Janeiro, Brazil.

Schoenemann, T., & Cremers, D. (2007b). Introducing curvature into globally optimimal image segmentation: minimum ratio cycles on product graphs. In *IEEE international conference on computer vision (ICCV)*. Rio de Janeiro, Brazil.

Sundaramoorthi, G., & Yezzi, A. J. (2005). More-than-topology-preserving flows for active contours and polygons. In *ICCV* (pp. 1276–1283).

Sundaramoorthi, G., Yezzi, A., & Mennucci, A. (2005). Sobolev active contours. In *VLSM* (pp. 109–120).

Sundaramoorthi, G., Jackson, J. D., Yezzi, A. J., & Mennucci, A. (2006). Tracking with Sobolev active contours. In *CVPR (1)* (pp. 674–680).

Sundaramoorthi, G., Yezzi, A., & Mennucci, A. (2007). Sobolev active contours. *International Journal of Computer Vision*, *73*(3), 345–366.

Sundaramoorthi, G., Yezzi, A., & Mennucci, A. (2008). Coarse-to-fine segmentation and tracking with Sobolev active contours. *IEEE Transactions on Pattern Analysis and Machine Intelligence*, *30*(5), 851–864.

Tsai, A., Yezzi, A. J., Tempany, W. M. W. C., III, Tucker, D., Fan, A., Grimson, W. E. L., & Willsky, A. S. (2001). Model-based curve evolution technique for image segmentation. In *CVPR (1)* (pp. 463–468).

Yezzi, A., & Mennucci, A. (2005a). Metrics in the space of curves. Preprint, arXiv:math.DG/0412454.

Yezzi, A. J., & Mennucci, A. (2005b). Conformal metrics and true "gradient flows" for curves. In *ICCV* (pp. 913–919).

Yezzi, A., Tsai, A., & Willsky, A. (1999). A statistical approach to snakes for bimodal and trimodal imagery. In *Int. conf. on computer vision* (pp. 898–903).

Zhu, S. C., Lee, T. S., & Yuille, A. L. (1995). Region competition: unifying snakes, region growing, energy/bayes/MDL for multi-band image segmentation. In *ICCV* (pp. 416).